18

Synchrotron Radiation: Applications in Diagnosis and Treatment of Malignant Brain Tumors

S. Kaiser Ali[1], Umashankar Das[2], Yanjie Lu[3], Vijayanada Kundapur[4] and Tim May[5]

[1]*College of Medicine, University of Saskatchewan, and Provincial Leader, Pediatric Oncology Program of Saskatchewan*

[2]*College of Pharmacy and Nutrition, University of Saskatchewan and Cancer Research Unit, Saskatchewan Cancer Agency*

[3]*Cancer Research Unit, Saskatchewan Cancer Agency*

[4]*College of Medicine, University of Saskatchewan, and Saskatoon Cancer Centre Saskatchewan Cancer Agency*

[5]*Canadian Light Source, University of Saskatchewan Canada*

1. Introduction

According to the reports published by the American Cancer Society, an estimated 22,020 cases of primary malignant tumors of brain and other central nervous system (CNS) sites were diagnosed in the United States in 2010 (Jemal et al. 2010, 277-300). During the same period, approximately 13,140 persons with these tumor types succumbed to their disease. Among adults, malignant brain tumors are estimated at 7.3 cases per 100,000 person-years, and in children 4.5 cases per 100,000 person-years (Maher and McKee 2010, 484-527). Malignant neoplasms of the brain and nervous system were estimated to have accounted for 1.5% of all new cancer cases and 2.3% of cancer deaths in the United States in 2008, as reported in the SEER Cancer Statistics Review (*Surveillance, Epidemiology, and End Results (SEER) Program,*
National Cancer Institute 1975-2005. www.seer.cancer.gov). Brain tumors aggregate in a bimodal age distribution pattern. The first occurs during infancy and early childhood between birth to 4 years of age, followed by a gradual rise in incidence after age 24, and a late second peak between 50–79 years of age. The Central Brain Tumor Registry of the United States reports that gliomas account for 36% of all primary brain tumors, and 81% of malignant tumors (*CBTRUS Statistical Report 2008: Primary brain tumors in the United States. Central brain tumor registry of the United States, Chicago. www. cbtrus.org)*. Among these, glioblastoma multiforme (GBM) is the most common (Raizer 2011, 152-157), accounting for at least 50% of cases. Glioblastoma multiforme remains an incurable disease, with a 5 year survival rate ranging from around 13% for patients aged 15-45 years to only 1% for those aged 75 years and older (*Surveillance, Epidemiology, and End Results (SEER) 2007, SEER* Stat software, version 6.3.5. www.seer.cancer.gov/seerstat/software*).

Obstacles to cure of brain tumors include, among others, the juxtaposition of tumor and vital centres of normal brain, "blood brain barrier"(Armulik et al. 2010, 557-561; Blanchette and Fortin 2011, 447-463; Kalra and Couldwell 2011, 179-180), limitations in achieving complete tumor resection, lack of concordance in tumor classification (Daumas-Duport and Varlet 2003, 622-636), and inherent resistance of untreated tumor to chemotherapy (Eimer et al. 2011, 1017-1027; Denysenko et al. 2010, 343-351; Luqmani 2005, 35-48), and radiation therapy (Friedman et al. 2009, 199-209). Newer approaches to investigating the biology of gliomas is the first step towards more precise identification of their dynamic evolution, which in turn should lead to development of more effective therapeutic strategies and improved long term survival.

2. Diagnosis of brain tumors

The World Health Organisation (WHO) Classification of Tumors of the CNS lists astrocytic tumors as the most common among tumors of neuroepithelial (or glial) tissue. The "gold standard" of this classification is a histopathological diagnosis based on light microscopy examination of hematoxylin and eosin (H&E) stained biopsy tissue sections. Slides are scanned to record gradation of tumor cell density, vascularisation, small-cell density and matrix loosening. Histologic grading of astrocytomas range from the most benign form (grade I - pilocytic astrocytomas) to the most malignant (grade IV – glioblastoma multiforme), based on the degree of anaplasia, mitotic index, degree of invasion into surrounding tissue, microvascular proliferation, and foci of necrosis (Kleihues et al. 2002, 215-25; Louis et al. 2007, 97-109). The term "multiforme" derives from the spectrum of different cell types and tissue heterogeneity observed within the tumor: astroblastic, oligodendroglial, and dedifferentiated cells in combination with anaplastic, gemistocytic, fibrillary, or pilocytic components (Iglesias-Rozas and Hopf 2005, 351-356).

However, subjectivity in interpretation and ambiguities in definitions and histologic criteria in the WHO classification (Tanaka et al. 2011; Reifenberger and Wesseling 2010, 549-551), such as multiple phenotypes within the same tumor at one or different points in time (Hassler et al. 2006, 46-55; Walker et al. 2003, 4841-4851) as well as newly-evolving tumor variants (Kozak and Moody 2009, 833-841; Valle-Folgueral et al. 2008, 343-349; Martinez et al. 2007, 26-34) and unclassifiable tumors (Cenacchi and Giangaspero 2004, 185-192) emphasize the limitations of histological classification.

Immunohistochemical stain panels provide more specific information regarding antigen expression associated with certain cell types, and also reflect patterns of genetic aberrations within tumors. These panels consist of a combination of immunoperoxidase stains and anti cellular-protein-specific monoclonal antibodies. Cytokeratins, vimentin, desmin, glial fibrillary acidic protein, and neurofilament protein stains serve to more accurately identify the cell lineage of tumors. In addition, immunocytochemical stains such as keratin, synaptophysin, S100, melanoma antigen recognized by T cells (MART-1), leukocyte common antigen (LCA), organic ion transporter 3/4 (OCT 3/4) and smooth muscle actin (SMA) provide a better definition in cases of less well-differentiated neoplasms (Wieczorek and Longtine 2010, 1-5). The advantage of these stains is that they can be used with paraffin-embedded stored tissue samples.

Increasingly, molecular biological and cytogenetic techniques are being used to investigate mechanisms of malignant transformation and to identify tumor markers predictive of behaviour and outcome (Martinez et al. 2007, 26-34; Krex et al. 2003, 1377-84). Aberrations

within the tumor genome have been detected by such molecular genetic techniques as fluorescent in-situ hybridisation, comparative genomic hybridisation (Wiltshire et al. 2000, 164-173), spectral karyotyping (Zuber et al. 2002, 111-115) and gene expression profiling (Liang et al. 2005, 5814-5819). Newer variants of "classical" GBM including giant cell, small cell, epitheloid, and rhabdoid variants, as well as those containing PAS and trichrome stain-positive intracellular inclusions, continue to manifest (Kleinschmidt-DeMasters et al. 2006, 273-286). These evolutionary changes in the histopathological manifestations of GBM are reflected in the 2007 revision of the original 2002 WHO classification, where newer GBM variants such as GBM with an oligodendroglioma component have been recognized (Nakamura, Makino, and Kuratsu 2011). Tumor heterogeneity detected by the array of these diagnostic methods is a compelling reason for developing more refined and accurate recognition techniques.

3. Fourier Transform (FTIR) Infrared Spectroscopy

The challenges posed by heterogeneous (Bleau, Huse, and Holland 2009, 2936-2944) expressions of histological, cytogenetic, and oncogenetic mechanisms within brain tumors can be addressed by a relatively new biodiagnostic research tool, vibrational spectroscopy.

Fourier Transform Infrared (FTIR) vibrational spectromicroscopy combines light microscopy with infrared spectroscopy. It uses mid-infrared light obtained from a conventional thermal source as a probe to characterise qualitative and quantitative vibrational properties of biological specimens at a molecular level. FTIR spectroscopy is both a chemical and a molecular probe. The infrared (IR) spectra generated by biological tissues are a composite display of vibrational shifts in covalent bonds, derived from their biomolecular content (proteins, lipids, sugars, and nucleic acids).

The intensities of the spectra express quantitative information, while the frequencies at which they are displayed reflect qualitative information on the nature, composition, and relationships of their molecular structures. FTIR data can therefore be used as molecular "fingerprints" for correlation of spectral patterns with biological structure unique to normal tissues and their malignant counterparts. The technique of FTIR has the advantage of examining tissues "at the source" and not requiring any processing of the samples prior to testing. Scientists have capitalised on the finding that lipid, protein, carbohydrate and nucleic acid content of biological tissues can be precisely identified by specific spectral "signatures" generated when they are subjected to absorption spectroscopy using mid-infrared (mid-IR) light (wave numbers 4000-1000 cm^{-1}) (Marinkovic et al. 2002, 189-197). The amide I band (~1650 cm^{-1}) results mainly from the ν(C=O) stretching vibrations of protein amide bonds. The amide II band ~ 1549 cm^{-1} arises from the *d*(N–H) bending and ν(C–N) stretching vibrations of amide bonds. The ν(C=O) stretching of lipids is displayed ~ 1740 cm^{-1}, and the anti-symmetric ν ($PO2^-$) stretching of nucleic acids and phospholipids ~ 1225 cm^{-1}.

The precise frequency of absorption from a particular molecular bond or group is dependent on the environment in which it resides; specific changes within them characterise such conditions as skin cancer (McIntosh et al. 1999, 951-956). The commencement of transformation of normal tissues into a dysplastic state, and onwards to neoplasia, is most likely initiated at a subcellular level by molecular changes and subtle shifts in tissue components, amenable to detection by IR spectromicroscopy. The subtle changes in large numbers of spectra generated during biospectroscopy are prone to subjective error if

interpreted by inspection alone. This problem can be overcome by means of multivariate statistical analyses performed by specific software programs designed for this purpose. FTIR spectromicroscopy is proving to be a useful complementary tool for purposes of enhanced diagnostic accuracy, improved tumor grading, developing treatment strategies, and monitoring responses to therapy.

3.1 Conventional FTIR - animal studies

In a study using FTIR imaging of C6 gliomas grown in the brains of Wistar rats, researchers were able to differentiate between normal brain structures and tumor tissue; altered patterns were detected in the intermediate zones. FTIR transmission spectroscopy confirmed decreased concentrations of lipids within tumors, which was correlated to the degree of myelination present. The spectroscopic findings correlated with light microcopy detection of myelin in healthy brain tissues using Luxol fast blue and Luxol fast blue-cresyl stains (Amharref et al. 2006, 892-899). Reflection/absorption IR spectromicroscopy studies were conducted on autopsied formalin-fixed de-paraffinised tumor tissue sections of rat C6 glioma allografted in Wistar rat brain. Spectral signatures from malignant tissue were compared with those of a normal control, and subjected to multivariate analyses. This allowed for generation of false-colour coded maps, comparing variations in lipoprotein composition. In contrast to the normal sample, tumor spectra displayed qualitative and quantitative variations in amide I and II bands pertaining to protein components (Bambery et al. 2006, 900-907). Another study with the same animal model and using transmission spectroscopy demonstrated several features of clinical relevance: i) spectral patterns of proteins and nucleic acids could be used to differentiate between normal, malignant, peri-tumoral and necrotic brain tissues, ii) the development of tumor was marked by a reduction in total lipid content (cholesterol, phosphatidyletanolamine, phosphatidyl-choline, and galactocerebroside), and iii) glioma tissues contained a high amount of sphingomyelin, nucleic acids, and oleic acids (Beljebbar et al. 2008, 8406-8415).

3.2 Conventional FTIR - human studies

A proof of concept diagnostic study using IR spectroscopy to classify biopsy specimens of 25 human brain tumors resulted in an overall 89% concordance with light microscopy re. WHO diagnosis and grading of astrocytic tumors (Steiner et al. 2003, 464-471). Researchers were able to identify changes within tumors in both the nature, and relative amounts, of brain lipids, including gangliosides and phospholipids. In view of the conundrum that conventional histological findings are not predictive of tumor behavior, correlation between histological diagnoses and FTIR spectroscopy was conducted in a few cases of human head and neck tumors (gingival squamous cell carcinoma and sarcomatoid carcinoma). In the former, high DNA, lipid and collagen components were detected; in the latter, similar findings also were documented, but in a heterogeneous distribution (Bruni et al. 2004, 19-26).

IR spectroscopy was used to differentiate normal brain from both *in vitro* glioblastoma cell lines as well as 56 tumor specimens from glioma patients. In normal control samples, molecular signatures demonstrated differences between white and grey matter, based on increased spectral endowments from lipids and cholesterol. As well, these researchers were able to demonstrate progressive decreases in brain lipids, inversely proportional to the degree of anaplasia (Krafft et al. 2004, 921-925). Characteristic IR spectral signatures of

disparate tissue types from multiple tissue sections of two brain tumors were used to develop a multivariate classification model. The model was based on linear discriminant analysis (LDA) and used to classify single IR spectra from 51 patients. Results of analysis using the LDA model revealed 100% accuracy with normal brain tissue (5 samples), 80% accuracy for grade III astrocytomas (15 samples), and 74.2% accuracy for grade IV/GBM (31 samples) (Krafft et al. 2006, 301-305). Extension of this methodology to the macroscopic imaging mode of three tumor sections of GBM from one patient resulted in spectra that were almost identical. However, when a supervised classification model based on the LDA algorithm was applied to the data, gradation of tumor content was suggestive of tissue sections being derived from intra-tumor, tumor margin, and extra-tumor locations respectively (Krafft et al. 2007, 1669-1677).

Meningiomas comprise a group of brain tumors with significant risks of recurrence and unpredictable outcomes (Drummond, Zhu, and Black 2004, 113-130). We investigated, by means of mid-infrared reflectance spectromicroscopy, a number of meningiomas to determine their spectral signatures, and to more accurately differentiate tumor tissue from normal control (Ali et al. 2008, 297-301). Briefly, brain tumor samples were obtained at elective surgery from four patients with meningiomas. A sample derived from histologically proven normal brain tissue at the periphery of resected margins in one patient served as control. Paired tumor tissue sections 5 micrometres in thickness were cut in a cryostat at –20°C. The first section was placed on a glass slide for H&E stain, and the section immediately was transferred onto an IR-reflective slide for spectromicroscopy. Concordance of tumor-bearing areas was achieved by means of a novel technique developed in our lab. It requires superimposing a digital tractile grid over paired H&E and IR tissue section images of tumor bearing areas within the tissue section that are demarcated by a pathologist, and then transferring matching grid coordinates onto the overview image generated by the spectromicroscope in the preparation of mid-IR spectroscopy (**Figures 1a, 1b and 1c**) (Ali et al. 2010, 857-860).

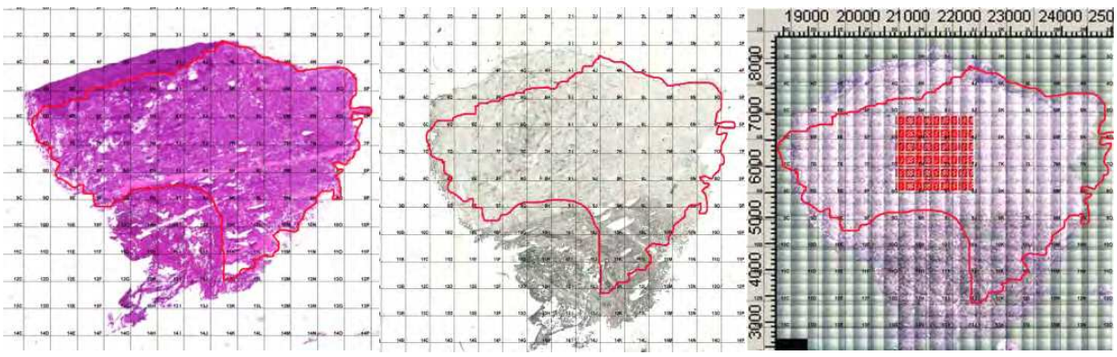

1a 1b 1c

Fig. 1. 1a. Equisized H&E stained tissue section with concordant grid and tumor-bearing area within digital boundaries (outlined in black). 1b. Equisized paired IR unstained tissue section showing tumor-bearing area (within red boundaries) with concordant grid and overlaid digital boundary map transferred from Figure 1a. Fig. 1c. Equisized spectromicroscopy overview image of tissue section with raster map (red square) outlined within tumor-bearing area (within red boundaries), in the preparation of mid-IR spectroscopy (note matched grid coordinates in all images).

Mid-IR microscopy data collection: Thin tumor section on the IR reflectance slide was raster scanned using Globar light-sourced spectromicroscopy at the Canadian Light Source (CLS) synchrotron facility. Spectromicroscopy was performed using an IFS 66v/S FTIR spectrometer with a conventional light source attached to a Hyperion IR microscope with a 15X Cassegrain objective and a single channel MCT detector. Raster scans were obtained in the mid-infrared range of 4000-900 cm^{-1} using a 50 micrometres x 50 micrometres aperture, 25 micrometres step size, 32 scans per step, and resolution of 4 cm^{-1}. Stage control, data collection and processing were done using OPUS software and analysed using CytoSpec, a software tool designed for FTIR image analysis. Visible images were obtained using a charged-couple device camera, which was linked to the infrared images.

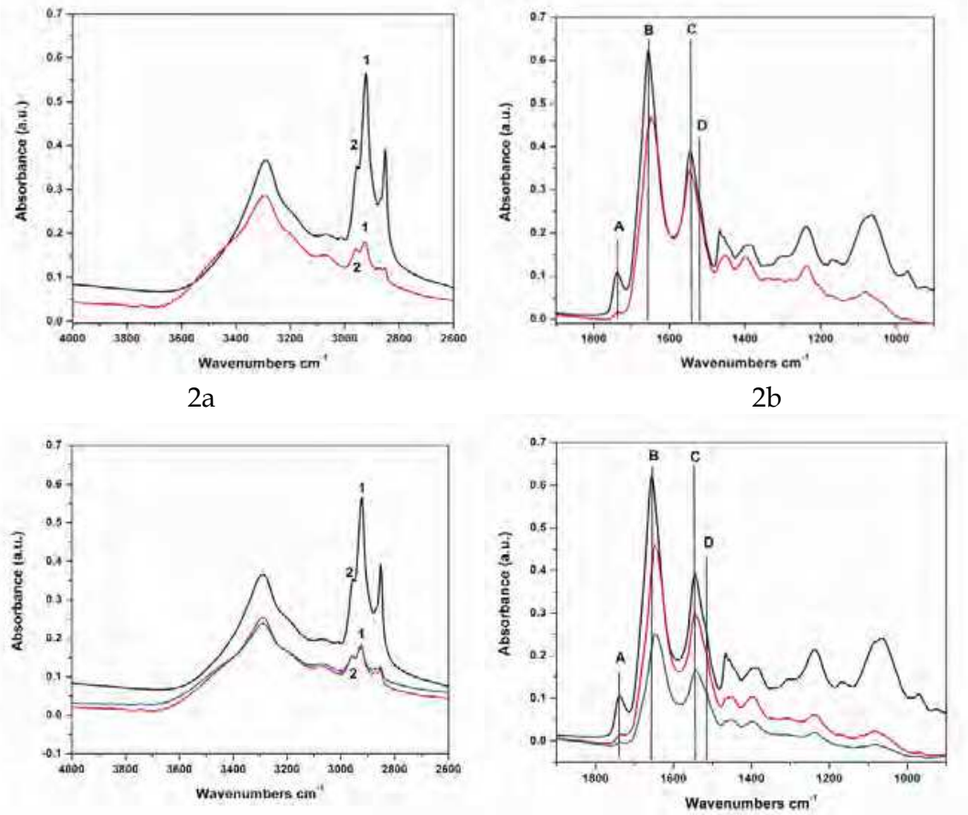

2a 2b

2c 2d

Fig. 2. Comparison of average mid-IR spectra of brain tissue samples, control and tumour in the spectral region of 4000-2600 cm^{-1} and 1900-900 cm^{-1}. 2a,b: Control spectrum (black) and a cluster from the tumour tissue (red). 2c,d: Control spectrum (black) and two clusters from the tumour tissue(red and blue). Despite similar spectra pattern in 2a-d, the following important points are noted. i) The relative CH_2 and CH_3 stretching intensities labeled as 1 and 2, respectively in 2a and 2c that represent lipid peaks are very different. ii) the peak A at 1735 cm^{-1} shows a large decrease in lipid concentrations in the tumour samples., iii) the peak B at 1655 cm^{-1} in 2c indicates the amide I peak in the tumour sample is largely unchanged from the control sample. This peak in 2d shifts towards 1631 cm^{-1}, iv) the peak C at 1548 cm^{-1} in 2c that represents protein amide II is largely unchanged from the control sample but this peak in 2d shifts slightly to 1544 cm^{-1}, and v) the peak D at 1515 cm^{-1} corresponds to tyrosine amidic linkage.

The average spectra shown in Figures **2a-d** compare two different brain tissue samples, control and tumor, each from a different patient.

The first, most striking difference occurs in the bands associated with lipids, particularly unsaturated fatty acids, demonstrating a marked decrease in all the clusters associated with tumor tissue. In particular, the bands at 3010, 2920, 2850, and 1735 cm^{-1} are all weaker than in the control spectra. More subtle differences are visible in the region between 1900-900 cm^{1}, particularly the among the protein bands. The amide I band of the control tissue shows a large proportion of undifferentiated proteins and a small contribution of α-helical proteins at 1655 cm^{-1}. The tumor tissue samples tend more towards undifferentiated proteins; however, some of the clusters show an increased beta-sheet band at 1631 cm^{-1}. A band associated with the amino acid tyrosine at 1515 cm^{-1} is generally more pronounced in the tumor samples than in the control samples. In the spectral region of 1500-900 cm^{-1}, the tumour samples shows very weak peak intensities compared to control.

The results to date indicate the presence of a unique signature that could help identify tumor tissue. The marked diminution of the bands associated with the lipids combined with subtle changes in the main protein bands seems to be an indicator that a sample tissue is derived from tumor. This fingerprint is similar for all the different samples studied to date, and it may be possible to refine this spectral fingerprint to detect to a specific tumour class. Comparable results were found in three other patients with meningiomas. One of the strengths of the study is that, in spite of small numbers, all four patients had the same type and grade of tumor confirmed by a pathologist. This avoided the potential problem arising from interpretation of disparate degrees of anaplasia within the same histological tumor type**.**

Fig. 3. SOLEIL synchrotron facility near Paris, France (Copyright © Synchrotron Soleil, reproduced with permission).

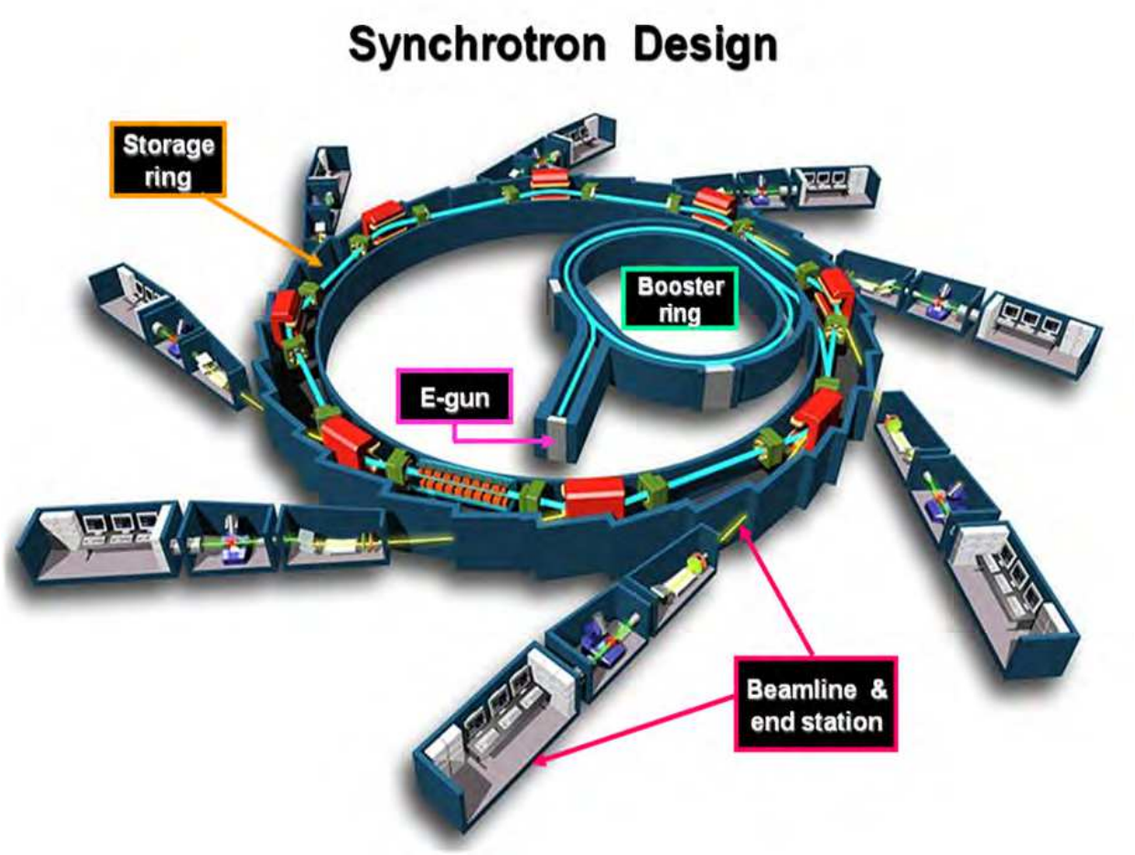

Fig. 4. Schematic diagram of Synchrotron Soleil. The circular ring is the synchrotron, a particle accelerator that brings electrons to very high speeds. The synchrotron emits "synchrotron radiation", especially X-rays; these are sent into the various beamlines (the straight lines branching out of the synchrotron). Each beamline contains scientific instruments, experiments etc. and receives an intense beam of radiation (Copyright © EPSIM 3D/JF Santarelli, Synchrotron Soleil, reproduced with permission).

4. Synchrotron

A synchrotron is a large ring-shaped particle accelerator into which electrons are fed from a smaller booster ring and a linear accelerator. The magnetic fields to turn the electrons, and electric fields to accelerate them within the main booster ring, are carefully synchronised with the electrons as they travel in a circular orbit at nearly the speed of light. The acceleration of electrons to this very high speed causes them to lose energy when they turn in magnetic fields. The energy is lost by emitting photons (light energy or electromagnetic radiation), which are then transported along tangential steel pipes called beamlines. The photon transport involves mirrors and devices for focusing and tuning the light for a particular use. The entire spectrum of electromagnetic radiation including, among others, (IR) Infrared light and monochromatic high energy x-ray beams, can be selectively extracted from photons within a given beamline and used for diagnostic and therapeutic applications (**Figure 5)**.

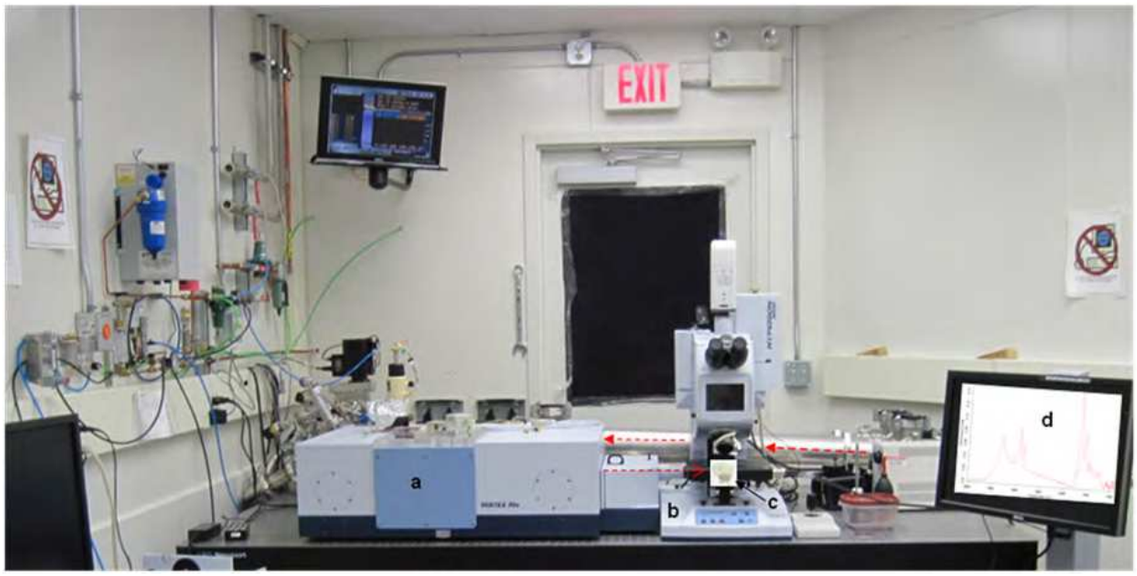

Fig. 5. Experimental hutch, 01B1-1 Mid-Infrared Spectromicroscopy beamline, Canadian Light Source, Saskatoon, Canada. Dotted arrows indicate pathway of synchrotron mid-IR beam entering spectrometer, passing through the tumour specimen, and generating the spectra. a. FTIR Spectrometer, b. spectromicroscope, c. unstained thin tumor section, d. spectra displayed on screen (author's files).

4.1 Synchrotron FTIR spectroscopy

Conventional thermal IR spectromicroscopy examination of biological tissues has limited spatial resolution, arising from low brightness diffraction or optical aberrations, including insufficient spatial resolution of only approximately 20-25 micrometres (Carr 2001, 1613). This problem is overcome by synchrotron IR light by virtue of its brightness, which is 100–1000 times greater than that from a conventional source (Miller and Dumas 2006, 846-857). Individual biological cells range from 5-30 micrometres in diameter, too small for probing by conventional IR sources. The much greater brightness of synchrotron-sourced light, however, permits intracellular imaging of molecular chemical structure and, compared to thermal IR light sources, provides greater spectroscopic detail and serves as a more refined diagnostic tool (Holman et al. 2002, 417-424) for a spectrum of malignant brain tumors, both in terms of differentiating tumor types as well as assessing degrees and patterns of anaplasia.

Figure 6 shows two absorbance spectra collected from 10 x 10 mm areas of the same region of a single tissue section. The upper trace was recorded using a synchrotron source, and the lower trace using a conventional thermal source. Each spectrum was collected for 1024 scans at 8 cm^{-1} spectral resolution. The advantage of the synchrotron as an infrared light source at high spatial resolution can clearly be seen in the difference between the spectra. The spectrum collected using the thermal source shows particularly high levels of "noise" in the fingerprint region below 1600 cm^{-1} (Tobin et al. 2004, 27-39).

It has become increasingly clear that synchrotron IR spectromicroscopy is an extremely valuable analytical tool when determining the chemical composition of biological and biomedical samples, at the diffraction-limited spatial resolution. Highly resolved IR spectromicroscopy, together with the high signal-to-noise level of recorded spectra, is

essential in generating chemical and statistically-derived multivariate images. Synchrotron IR spectromicroscopy is very useful because of the achievable diffraction-limited spatial resolution, for the high signal-to-noise spectra obtained even with a diffraction-limited spot size, and for rapid data acquisition. Details of the secondary (alpha-helix) structure of proteins and their intracellular distribution can be identified with much greater clarity, allowing detailed analysis because of good spectral quality. The synchrotron source provides the necessary brightness to fulfill this requirement in the case of individual cells (Dumas et al. 2004, 289-302).

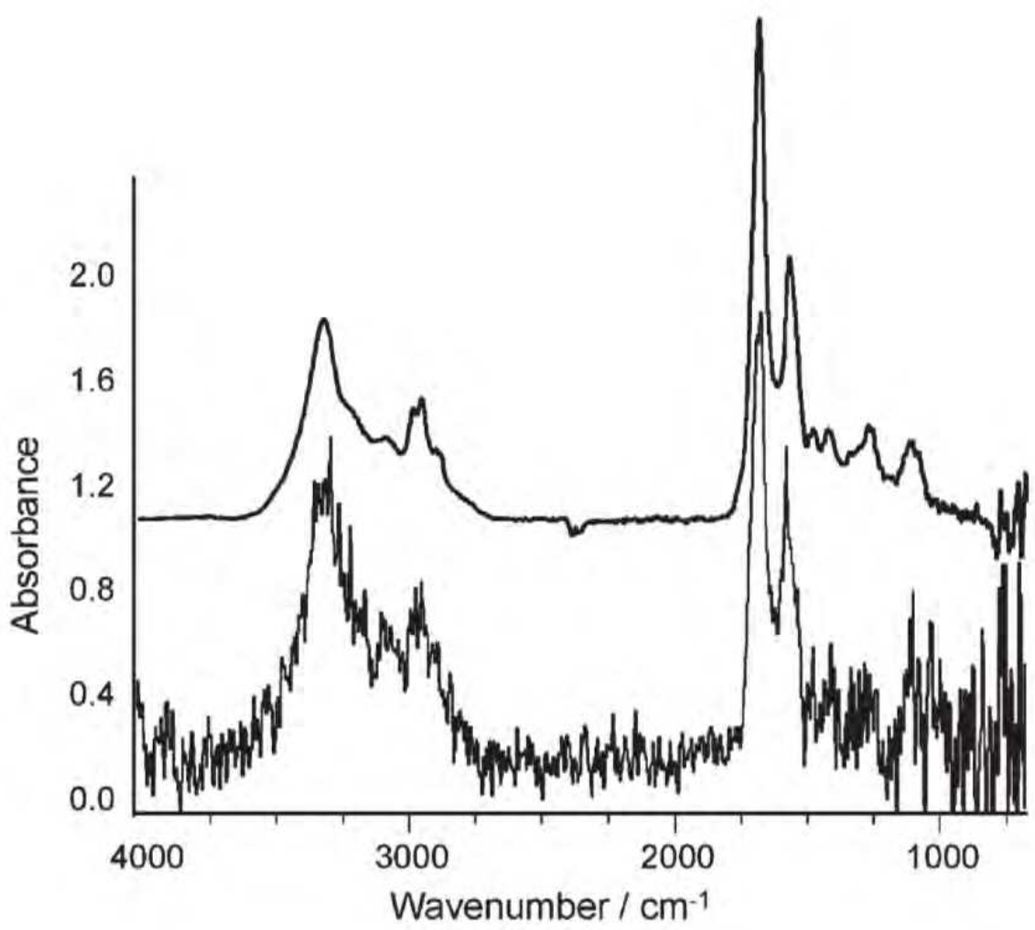

Fig. 6. Absorption spectra of tissue sample recorded under identical collection conditions using a thermal infrared source (lower trace) and synchrotron radiation (upper trace). (Copyright © The Royal Society of Chemistry, reproduced with permission)

Our diagnostic experiments progressed from using thermal light-sourced mid-IR reflectance spectromicroscopy to synchrotron light-sourced transmission spectromicroscopy to study human GBM tumor samples (Ali et al. 2010, 11-16). Tumor tissue was obtained from six patients with GBM and control samples from two other non-malignant patients. Experimental procedures were the same as for the meningioma study described earlier, with the following changes: The second of thin, paired tissue sections was mounted onto a CaF_2 slide for mid-IR transmission spectromicroscopy at the 01B1-1 beamline, Canadian Light

Source (CLS). Transmission spectromicroscopy was performed using a 36X Cassegrain objective and a single channel MCT detector. Raster scans were obtained in the range of 4000-900 cm^{-1} using a 10 x 10 micrometres aperture, 10 micrometres step size, 32 scans per step, and resolution of 4 cm^{-1}. A multivariate statistical analysis was performed after converting all spectra to their second derivative and subjecting them to hierarchical cluster analysis (HCA). Pseudo-color maps based on cluster analysis were then created by assigning a color to each spectral cluster.

A total of 16 raster maps of GBM tumour tissue specimens from 6 patients were obtained and the results compared with 7 maps of control brain tissue specimens from resection margins of two patients, one with craniopharyngioma and the other with astrocytic gliosis. A study pathologist confirmed normal brain tissue on histopathological examination of the two control samples. The average spectra of GBM and normal control tissues were generated using synchrotron-sourced mid-IR beamline at CLS (Figure 7)

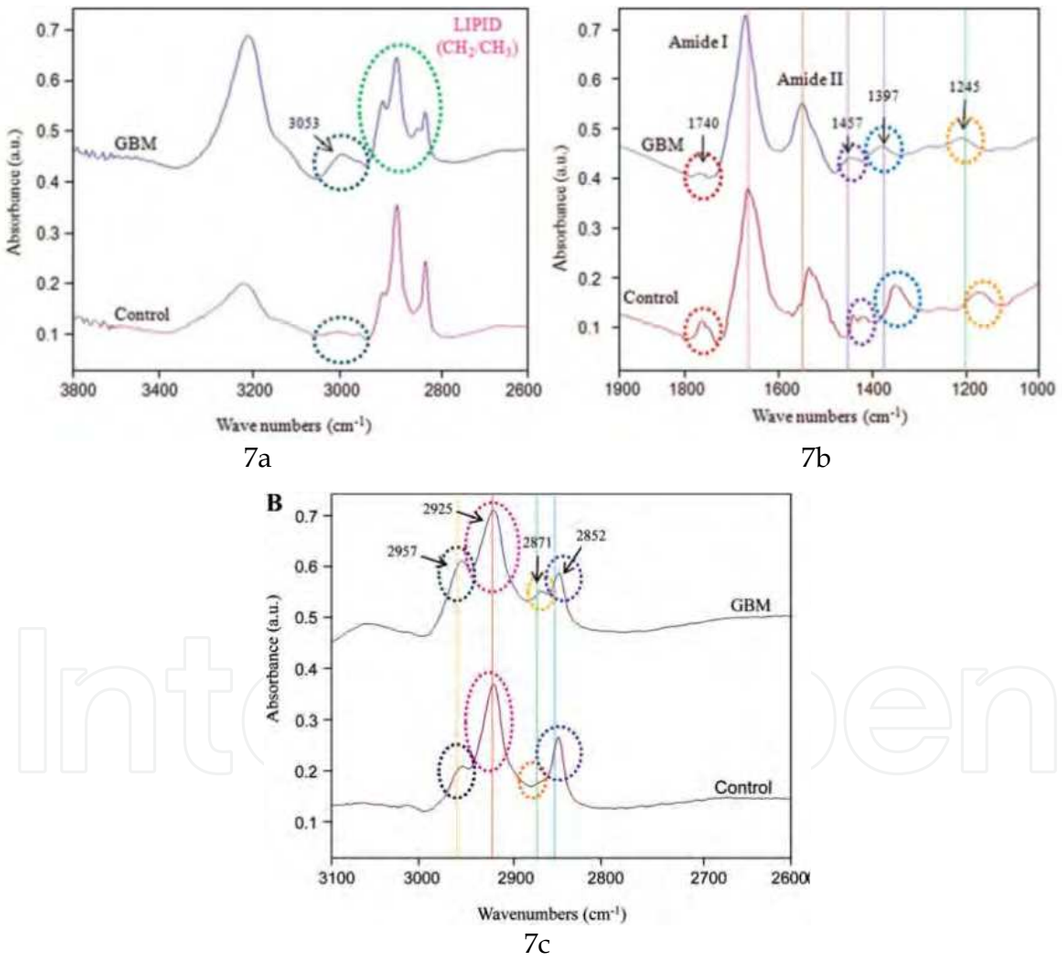

7a 7b

7c

Fig. 7. Comparison of average mid-IR spectra of GBM and control sample in the region of 3,800-2,600 (7a) and 1,900-900 cm^{-1} representing acyl vibrations fatty acids, peptide linkages of proteins, phosphodioxy groups of nucleic acids (7b) and the figure 7c depicts striking differences in the average spectra of GBM tumour and normal tissue in the spectral range of 3,100-2,600 cm^{-1}, representing lipid CH_2 and CH_3 stretching intensities.

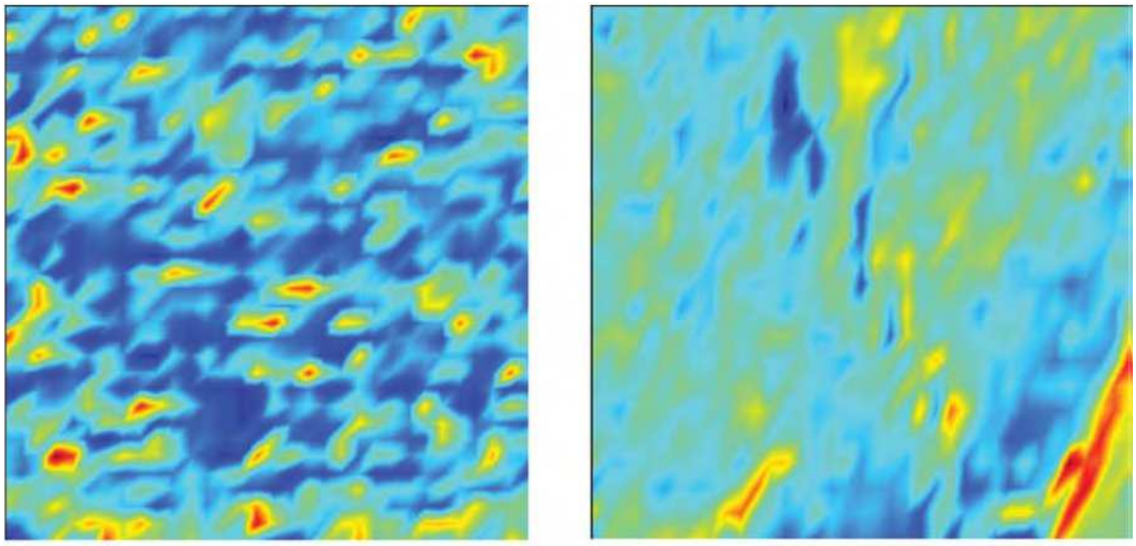

8a 8b

Fig. 8. Spectromicroscopic infrared mapping of tissue sections. False color codes represent varying tissue composition. 8a. Control, specimen displays four different clusters of spectra representing different tissue components. Blue and green pixels represent lipid and protein respectively; yellow & red pixels indicate nucleic acid components. 8b. GBM, displays marked reduction in lipid component.

The coloured cluster map representing control tissue (**Figure 8a**) clearly reflects four groupings of chemical moieties in normal brain tissue, including lipids, proteins, and nucleic acids. Blue pixels indicating lipid predominate; green and red pixel clusters indicate protein and DNA respectively. By contrast, in a GBM tumor sample (**Figure 8b**); lipid content is reduced drastically while protein content comprises the major portion of the image.

Data obtained from spectral comparisons of tumor and control samples graphically display spatial distribution of cluster groups representing different tissue components. **Figure 9** demonstrates false colour images displaying the spatial distribution of clusters from our experiments. Five clusters were considered for both control and tumour tissues. Each cluster was assigned a false color code for comparison purposes. The images in **Figures 9a and 9b**, representing control and GBM specimens respectively, clearly differentiate between the spatial distribution of the various clusters identified by the hierarchical cluster analysis (HCA) algorithm (Ward's algorithm). In GBM tumour samples, the cluster representing red pixels, most likely lipid, has been significantly reduced, while clusters identified by green pixels predominate, compared to control sample. These false colour cluster images demonstrate the sensitivity of these HCA method techniques in displaying subtle differences not obvious on visual inspection alone. A number of significant differences in the mid-IR spectral patterns of have been identified in GBM tumours compared to normal brain tissue. These differences could serve as diagnostic molecular spectral "signatures" in identifying residual GBM within tumour resection margins. A further study with larger number of patient samples for precise identification of a molecular signature unique to GBM has corroborated the spectral signatures identified in our pilot study (manuscript in preparation).

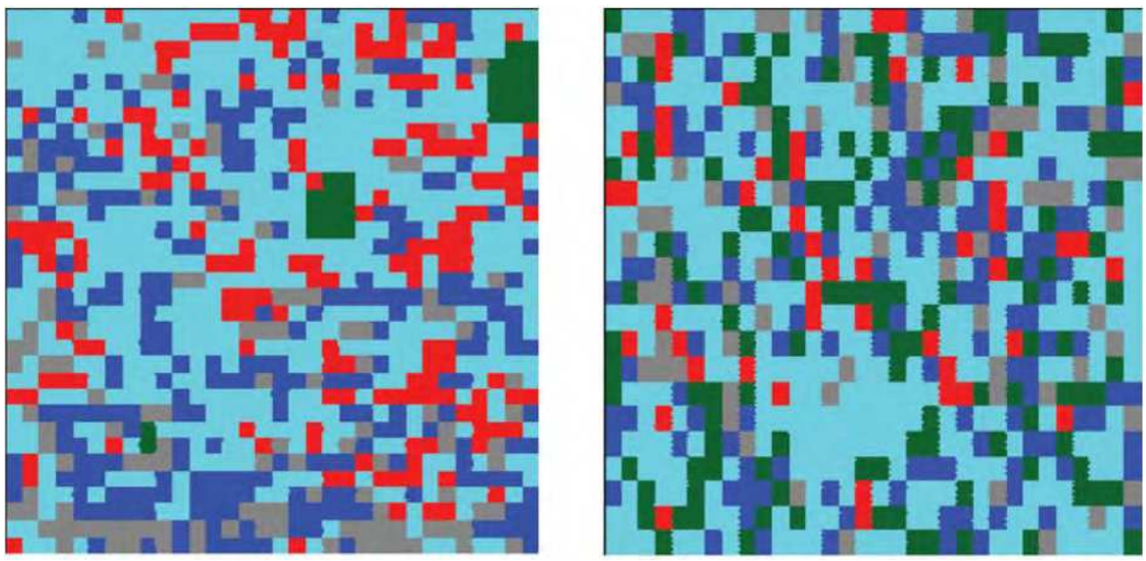

9a 9b

Fig. 9. Hierarchical (HCA) cluster analysis of (9a) control specimen and (9b) GBM tumor specimen. HCA false color image of 5 clusters displaying diversity in tissue composition of tumor tissue compared to control (see below).

4.2 Synchrotron Microbeam Radiation Therapy (MRT)

Curative management of human brain tumors is dependent upon accuracy of histological diagnosis and grading, achieving tumor-free margins during surgical removal, and inclusion of residual macroscopic and microscopic tumor within radiation therapy fields (Mason et al. 2007, 110-117) (Brem et al. 2011, 352-400). Obstacles to cure of a highly anaplastic tumor like GBM include inability to achieve complete tumor resection because of its rapid growth and invasive properties, migration of GBM cells several centimeters away from the primary tumor and even into the contralateral cerebral hemisphere (Lefranc, Brotchi, and Kiss 2005, 2411-2422), and its inherent resistance to radiation therapy and chemotherapy (Kemper et al. 2004, 415-423). Newer, innovative, and more precisely-targeted treatment approaches are required to positively impact on survival.

One of the limiting factors in delivery of curative radiation therapy to cancer patients is the dose-limiting tolerance of normal tissues (Deman et al. 2010, 586-589). There are several promising treatment approaches (Clarke, Butowski, and Chang 2010, 279-283) aimed at increasing the survival rate for patients with GBM tumors. One such therapy is microbeam radiation therapy (MRT), which has been designed for the specific purpose of maximising tumoricidal dose delivery while sparing surrounding normal tissues (Regnard et al. 2008, 861-878; Dilmanian et al. 2006, 9709-9714; Nettelbeck et al. 2009, 447-456; Serduc et al. 2009, 6711-6724; Prezado et al. 2009, 4897-4902).

Synchrotron-generated parallel, planar, micrometre-wide X-ray beams (microbeams) have been shown to safely deliver significantly higher than normal doses to the cerebella of weaning piglets without obvious neurological deficit one year later (Figure 10) (Laissue et al. 2007, 577-581). Histopathological examination at autopsy revealed preservation of normal cerebellar architecture except for thin, white horizontal parallel stripes approximately 20-30 micrometres in width, corresponding to the path of the microbeams. Degenerative changes

in neurons and astroglial cells were noted only along the tracks of the microbeams; no tissue necrosis, hemorrhage or demyelination were noted by light microscopy. This leads the way for MRT as a potential tool to treat brain tumors in young children, whose CNS is still in the developmental stages and therefore vulnerable to compromise of neurocognitive functions.

Fig. 10. Cerebellum of a piglet about 15 months after irradiation (skin entrance dose 300 Gy); hematoxylin/eosin-stained horizontal tissue section. Tissue has maintained its normal architecture. This white horizontal parallel stripes, clearly visible in inset, correspond to paths of approximately 27 μM-wide microbeam; beam spacing was about 210 μM (Copyright © Developmental Medicine & Child Neurology, reproduced with permission)

The concept of MRT is similar to GRID therapy (Tenzel 1952, 399-408; Huhn et al. 2006, 607-612; Mohiuddin et al. 1999, 721-727) in that healthy tissue is spared by applying discretely spaced beams as opposed to a continuous solid beam over the same volume. With MRT, several narrow beams tens of micrometres in width, spaced hundreds of micrometres apart, are delivered through the tumor. With high dose rates, these beams have been shown to preferentially kill glioblastoma tumors while better sparing the healthy brain tissues (Deman et al. 2010, 586-589; Sheleg et al. 2002, 53-59; Miura et al. 2006, 71-75; Dilmanian et al. 2003, 632-641). Although the mechanism of action of MRT remains to be elucidated, there are indications that the vasculature damaged by MRT is more readily repaired in healthy tissue than in glioblastoma tumors. This purported repair mechanism is felt to be dependent on differential regenerative activity of capillary endothelial cells in spared tissues in between the microbeams. Until now, MRT research has been carried out primarily at a

limited number of international synchrotron facilities. The main advantage of a synchrotron-derived radiation source is a very high dose rate, at least several hundred Gy per second, which allows for near instantaneous treatment times. This is important when dealing with micrometre-sized beams. If treatment times are drawn out, the energy deposited by the microbeams is spread out due to vascular pulsations and organ motion. Another advantage of a synchrotron source is that it is essentially nondivergent. This allows for the production of very flat minibeam profiles with little offaxis fall off. Nondivergent beams also yield a sharper penumbra on the individual minibeams, which in turn yields lower valley doses. While awaiting validation of proven safety and efficacy, synchrotron MRT treatment studies to date have been restricted to *in vitro* and *in vivo* pre-clinical experiments, mostly with brain tumors grown in small animals.

In preparation for synchrotron MRT experiments, we designed and created a minibeam collimator for minibeam radiation therapy studies in rodents using a 250 kVp clinical X-ray machine as a simulated synchrotron source (Babcock et al. 2011, 2192-2197). Our research has been designed to lead up to pre-clinical studies using synchrotron MRT. We have established an animal model of GBM xenografts grown in brains of immunocompromised nude mice, and plan to commence studies at the Biomedical Imaging and Therapy (BMIT) beamline 05B1-1 at the Canadian Light Source (CLS). The CLS is Canada's national synchrotron facility, located on campus at the University of Saskatchewan (Wysokinski et al. 2007, 73-76).

A treatment strategy designed to overcome limitations in tissue radiation tolerance was studied in a rat F98 glioma model. Test animals with implanted brain tumor were treated with a synergistic combination of single dose beam synchroton radiation, simultaneous with an infusion of an iodinated contrast agent. The results were compared with two other control groups: untreated tumor-bearing rats, and those treated with synchrotron radiation therapy alone. A 20% and 44% increase in life spans were noted in the rats irradiated without or with iodine, respectively, albeit a modest one in terms of days of prolongation of life (median survival times of 12.5, 15 and 18 days for untreated controls, irradiated without iodine, or with iodine respectively)(Adam et al. 2003, 1413-1426). The research group developed a strategy aimed at disrupting the blood-brain barrier to increase delivery of iodinated contrast agent into F98 rat gliomas.

The blood-brain barrier (BBB) is an integrated physiological system composed of interdigitating endothelial cells supported by pericytes, astrocytes and extracellular matrix, as well as enzymes, and transporters, working in concert to maintain homeostasis of the extracellular milieu. In so doing, it impedes the transport of chemotherapeutic agents across the vascular compartment into the CNS matrix. Osmotic disruption of the BBB is achieved by administration of hypertonic solutions such as mannitol, which induce crenation of the endothelial cells, disruption of their tight interdigitations, and enhanced diffusion of drugs across the BBB (Kemper et al. 2004a, 415-423). In principle, osmotic disruption of the BBB should allow for increased deposition of radiosensitising agents within tumor, thereby increasing the total lethal dose of intra-tumoral irradiation following external beam radiation treatment.

In the next series of experiments in F98 glioma-bearing rats were treated with synchrotron stereotactic radiotherapy (SSR) in a single dose fraction, simultaneous with intravascular infusion (intra-arterial or intravenous) of a combination of iodinated contrast agent and mannitol. The latter drug was added to induce temporary BBB disruption and thereby allow greater deposition of photoactive contrast within the tumor while it was being irradiated.

Percentage increase in life span (ILS) was most significant (169%) in rats who received both SSR and combined drugs via intra-arterial (i.e., intra-carotid) administration for X-ray doses ≤ 15 Gy. Administration via the intravenous route of the same drug combination concomitant with SSR resulted in 116% ILS, while no benefit was noted (91% ILS) in the group treated with SSR only. Of interest is the fact that at 25 Gy dose, survival advantage was greatest in the group that was treated with SSR alone (Adam et al. 2006, 603-611).

Furthering the above studies, a platinum derivative, *cis*-Platinum (CDDP), was chosen to explore the synergistic effect of platinum compounds reported in human studies. Interestingly, this pioneering study (Biston et al. 2004, 2317-2323) showed more than twice the amount of double-strand breaks (DSB's) when mouse models were treated with a combination of CDDP and synchrotron beam radiation with energy in the vicinity of platinum K-edge. The study also correlated survival benefit compared to other energy beams.

Realisation that modulation of energy of electromagnetic beams given in combination with compounds that achieve supra-additive tumor ablation (De Stasio et al. 2006, 206-213), while sparing normal tissues, creates possibilities for ambitious research undertakings. Further understanding of this as yet unchartered territory will pave the way for developing novel treatment methods resulting in enduring control of these tumors.

5. Conclusions

Histological grading of tumors delineates a continuum from least to most malignant (grade I-IV, respectively). Gradations of malignancy, as well as variations in tumor type, may be identified in a single tissue section. The challenge for the pathologist lies in accurately identifying the tumor and assessing the degree of anaplasia in order to guide the clinician with information to optimise treatment strategy and obtain a favourable outcome.

Malignant tumors can be considered reverse versions of their tissues of origin, endowed with the ability to continually evolve their cellular structure and extracellular matrix in response to changes in their microenvironment. Diagnostic light microscopy examination and immunohistochemical stains identify events "frozen" at one point in time, i.e., when the tumor is biopsied or excised. As we begin to consider and understand tumors more as dynamic entities, our approach to studying their biologic behavior by conventional static diagnostic methodologies is increasingly being supplemented by biochemical, molecular genetic, and cell signaling probes. IR spectroscopy serves as a light probe, penetrating tissues and cells at a molecular level, in real time, to provide a composite display of the chemical composition and molecular structural relationships of tissues and individual cells.

The brilliant intensity of synchrotron-generated light energy, a form of electromagnetic radiation, reveals nuances of tumor tissue activity at a subcellular or molecular level. It "illumines" our minds to the understanding that tissues, normal and malignant, even when completely severed from the body, can still dance to a rhythm of inherent vibrations that identifies them as unique. Another form of synchrotron-sourced electromagnetic radiation, microbeam radiations, proves a tool for improved eradication of malignant tumors, which are themselves none other than condensed forms of electromagnetic radiations. Thus, in the domain of brain tumors, the synchrotron serves a triple purpose as a diagnostic, treating, and teaching tool.

6. Acknowledgement

Our research work described in this paper was funded by a peer-reviewed grant from the Saskatchewan Cancer Agency, and by a grant from office of the Vice-President, Research, College of Medicine, University of Saskatchewan. Research described in this paper was performed at the Canadian Light Source, which is supported by the Natural Sciences and Engineering Research Council of Canada, the National Research Council Canada, the Canadian Institutes of Health Research, the Province of Saskatchewan, Western Economic Diversification Canada, and the University of Saskatchewan.
http://www.lightsource.ca/uso/publications.php

7. References

Adam, J. F., H. Elleaume, A. Joubert, M. C. Biston, A. M. Charvet, J. Balosso, J. F. Le Bas, and F. Esteve. 2003. Synchrotron radiation therapy of malignant brain glioma loaded with an iodinated contrast agent: First trial on rats bearing F98 gliomas. *International Journal of Radiation Oncology, Biology, Physics* 57 (5) (Dec 1): 1413-26.

Adam, J. F., A. Joubert, M. C. Biston, A. M. Charvet, M. Peoc'h, J. F. Le Bas, J. Balosso, F. Esteve, and H. Elleaume. 2006. Prolonged survival of fischer rats bearing F98 glioma after iodine-enhanced synchrotron stereotactic radiotherapy. *International Journal of Radiation Oncology, Biology, Physics* 64 (2) (Feb 1): 603-11.

Ali, K., Y. Lu, C. Christensen, T. May, C. Hyett, R. Griebel, D. Fourney, K. Meguro, L. Resch, and R. K. Sharma. 2008. Fourier transform infrared spectromicroscopy and hierarchical cluster analysis of human meningiomas. *International Journal of Molecular Medicine* 21 (3) (Mar): 297-301.

Ali, K., Y. Lu, U. Das, R. K. Sharma, S. Wiebe, K. Meguro, V. Sadanand, et al. 2010. Biomolecular diagnosis of human glioblastoma multiforme using synchrotron mid-infrared spectromicroscopy. *International Journal of Molecular Medicine* 26 (1) (Jul): 11-6.

Ali, K., T. Reichert, D. Gomez, Y. Lu, A. Jan, and C. Christensen. 2010. A new approach to concordance in mid-infrared spectromicroscopy mapping of malignant tumors. *Oncology Reports* 24 (4) (Oct): 857-60.

Amharref, N., A. Beljebbar, S. Dukic, L. Venteo, L. Schneider, M. Pluot, R. Vistelle, and M. Manfait. 2006. Brain tissue characterisation by infrared imaging in a rat glioma model. *Biochimica Et Biophysica Acta* 1758 (7) (Jul): 892-9.

Armulik, A., G. Genove, M. Mae, M. H. Nisancioglu, E. Wallgard, C. Niaudet, L. He, et al. 2010. Pericytes regulate the blood-brain barrier. *Nature* 468 (7323) (Nov 25): 557-61.

Babcock, K., N. Sidhu, V. Kundapur, and K. Ali. 2011. Collimator design for experimental minibeam radiation therapy. *Medical Physics* 38 (4) (Apr): 2192-7.

Bambery, K. R., E. Schultke, B. R. Wood, S. T. Rigley MacDonald, K. Ataelmannan, R. W. Griebel, B. H. Juurlink, and D. McNaughton. 2006. A fourier transform infrared microspectroscopic imaging investigation into an animal model exhibiting glioblastoma multiforme. *Biochimica Et Biophysica Acta* 1758 (7) (Jul): 900-7.

Beljebbar, A., N. Amharref, A. Leveques, S. Dukic, L. Venteo, L. Schneider, M. Pluot, and M. Manfait. 2008. Modeling and quantifying biochemical changes in C6 tumor gliomas by fourier transform infrared imaging. *Analytical Chemistry* 80 (22) (Nov 15): 8406-15.

Biston, M. C., A. Joubert, J. F. Adam, H. Elleaume, S. Bohic, A. M. Charvet, F. Esteve, N. Foray, and J. Balosso. 2004. Cure of fisher rats bearing radioresistant F98 glioma treated with cis-platinum and irradiated with monochromatic synchrotron X-rays. *Cancer Research* 64 (7) (Apr 1): 2317-23.

Blanchette, M., and D. Fortin. 2011. Blood-brain barrier disruption in the treatment of brain tumors. *Methods in Molecular Biology (Clifton, N.J.)* 686 : 447-63.

Bleau, A. M., J. T. Huse, and E. C. Holland. 2009. The ABCG2 resistance network of glioblastoma. *Cell Cycle (Georgetown, Tex.)* 8 (18) (Sep 15): 2936-44.

Brem, S. S., P. J. Bierman, H. Brem, N. Butowski, M. C. Chamberlain, E. A. Chiocca, L. M. Deangelis, et al. 2011. Central nervous system cancers. *Journal of the National Comprehensive Cancer Network : JNCCN* 9 (4) (Apr): 352-400.

Bruni, P., C. Conti, E. Giorgini, M. Pisani, C. Rubini, and G. Tosi. 2004. Histological and microscopy FT-IR imaging study on the proliferative activity and angiogenesis in head and neck tumours. *Faraday Discussions* 126: 19-26.

Carr, GL. 2001. Resolution limits for infrared microspectroscopy explored with synchrotron radiation. *Review of Scientific Instruments* 72 : 1613-9.

Cenacchi, G., and F. Giangaspero. 2004. Emerging tumor entities and variants of CNS neoplasms. *Journal of Neuropathology and Experimental Neurology* 63 (3) (Mar): 185-92.

Clarke, J., N. Butowski, and S. Chang. 2010. Recent advances in therapy for glioblastoma. *Archives of Neurology* 67 (3) (Mar): 279-83.

Daumas-Duport, C., and P. Varlet. 2003. Dysembryoplastic neuroepithelial tumors. *Revue Neurologique* 159 (6-7 Pt 1) (Jul): 622-36.

De Stasio, G., D. Rajesh, J. M. Ford, M. J. Daniels, R. J. Erhardt, B. H. Frazer, T. Tyliszczak, et al. 2006. Motexafin-gadolinium taken up in vitro by at least 90% of glioblastoma cell nuclei. *Clinical Cancer Research : An official Journal of the American Association for Cancer Research* 12 (1) (Jan 1): 206-13.

Deman, P., M. Edouard, S. Besse, M. Vautrin, H. Elleaume, J. F. Adam, and F. Esteve. 2010. Synchroton radiotherapy (*La Revue De Medecine Interne)* 31 (8) (Aug): 586-9.

Denysenko, T., L. Gennero, M. A. Roos, A. Melcarne, C. Juenemann, G. Faccani, I. Morra, et al. 2010. Glioblastoma cancer stem cells: Heterogeneity, microenvironment and related therapeutic strategies. *Cell Biochemistry and Function* 28 (5) (Jul): 343-51.

Dilmanian, F. A., G. M. Morris, N. Zhong, T. Bacarian, J. F. Hainfeld, J. Kalef-Ezra, L. J. Brewington, J. Tammam, and E. M. Rosen. 2003. Murine EMT-6 carcinoma: High therapeutic efficacy of microbeam radiation therapy. *Radiation Research* 159 (5) (May): 632-41.

Dilmanian, F. A., Z. Zhong, T. Bacarian, H. Benveniste, P. Romanelli, R. Wang, J. Welwart, T. Yuasa, E. M. Rosen, and D. J. Anschel. 2006. Interlaced x-ray microplanar beams: A radiosurgery approach with clinical potential. *Proceedings of the National Academy of Sciences of the United States of America* 103 (25) (Jun 20): 9709-14.

Drummond, K. J., J. J. Zhu, and P. M. Black. 2004. Meningiomas: Updating basic science, management, and outcome. *The Neurologist* 10 (3) (May): 113-30.

Dumas, P., N. Jamin, J. L. Teillaud, L. M. Miller, and B. Beccard. 2004. Imaging capabilities of synchrotron infrared microspectroscopy. *Faraday Discussions* 126: 289-302.

Eimer, S., M. A. Belaud-Rotureau, K. Airiau, M. Jeanneteau, E. Laharanne, N. Veron, A. Vital, H. Loiseau, J. P. Merlio, and F. Belloc. 2011. Autophagy inhibition cooperates

with erlotinib to induce glioblastoma cell death. *Cancer Biology & Therapy* 11 (12) (Jun 15): 1017-27.

Friedman, G. K., C. P. Langford, J. M. Coleman, K. A. Cassady, J. N. Parker, J. M. Markert, and G. Yancey Gillespie. 2009. Engineered herpes simplex viruses efficiently infect and kill CD133+ human glioma xenograft cells that express CD111. *Journal of Neuro-Oncology* 95 (2) (Nov): 199-209.

Hassler, M., S. Seidl, B. Fazeny-Doerner, M. Preusser, J. Hainfellner, K. Rossler, D. Prayer, and C. Marosi. 2006. Diversity of cytogenetic and pathohistologic profiles in glioblastoma. *Cancer Genetics and Cytogenetics* 166 (1) (Apr 1): 46-55.

Holman, H. Y., K. A. Bjornstad, M. P. McNamara, M. C. Martin, W. R. McKinney, and E. A. Blakely. 2002. Synchrotron infrared spectromicroscopy as a novel bioanalytical microprobe for individual living cells: Cytotoxicity considerations. *Journal of Biomedical Optics* 7 (3) (Jul): 417-24.

Huhn, J. L., W. F. Regine, J. P. Valentino, A. S. Meigooni, M. Kudrimoti, and M. Mohiuddin. 2006. Spatially fractionated GRID radiation treatment of advanced neck disease associated with head and neck cancer. *Technology in Cancer Research & Treatment* 5 (6) (Dec): 607-12.

Iglesias-Rozas, J. R., and N. Hopf. 2005. Histological heterogeneity of human glioblastomas investigated with an unsupervised neural network (SOM). *Histology and Histopathology* 20 (2) (Apr): 351-6.

Jemal, A., R. Siegel, J. Xu, and E. Ward. 2010. Cancer statistics, 2010. *CA: A Cancer Journal for Clinicians* 60 (5) (Sep-Oct): 277-300.

Kalra, R., and W. T. Couldwell. 2011. Regulation of the blood-brain barrier: New treatments for central nervous system neoplasms. *World Neurosurgery* 75 (2) (Feb): 179-80.

Kemper, E. M., W. Boogerd, I. Thuis, J. H. Beijnen, and O. van Tellingen. 2004a. Modulation of the blood-brain barrier in oncology: Therapeutic opportunities for the treatment of brain tumours? *Cancer Treatment Reviews* 30 (5) (Aug): 415-23.

Kleihues, P., D. N. Louis, B. W. Scheithauer, L. B. Rorke, G. Reifenberger, P. C. Burger, and W. K. Cavenee. 2002. The WHO classification of tumors of the nervous system. *Journal of Neuropathology and Experimental Neurology* 61 (3) (Mar): 215-25.

Kleinschmidt-DeMasters, B. K., L. Meltesen, L. McGavran, and K. O. Lillehei. 2006. Characterization of glioblastomas in young adults. *Brain Pathology (Zurich, Switzerland)* 16 (4) (Oct): 273-86.

Kozak, K. R., and J. S. Moody. 2009. Giant cell glioblastoma: A glioblastoma subtype with distinct epidemiology and superior prognosis. *Neuro-Oncology* 11 (6) (Dec): 833-41.

Krafft, C., S. B. Sobottka, K. D. Geiger, G. Schackert, and R. Salzer. 2007. Classification of malignant gliomas by infrared spectroscopic imaging and linear discriminant analysis. *Analytical and Bioanalytical Chemistry* 387 (5) (Mar): 1669-77.

Krafft, C., S. B. Sobottka, G. Schackert, and R. Salzer. 2004. Analysis of human brain tissue, brain tumors and tumor cells by infrared spectroscopic mapping. *The Analyst* 129 (10) (Oct): 921-5.

Krafft, C., K. Thummler, S. B. Sobottka, G. Schackert, and R. Salzer. 2006. Classification of malignant gliomas by infrared spectroscopy and linear discriminant analysis. *Biopolymers* 82 (4) (Jul): 301-5.

Krex, D., B. Mohr, H. Appelt, H. K. Schackert, and G. Schackert. 2003. Genetic analysis of a multifocal glioblastoma multiforme: A suitable tool to gain new aspects in glioma development. *Neurosurgery* 53 (6) (Dec): 1377-84.

Laissue, J. A., H. Blattmann, H. P. Wagner, M. A. Grotzer, and D. N. Slatkin. 2007. Prospects for microbeam radiation therapy of brain tumours in children to reduce neurological sequelae. *Developmental Medicine and Child Neurology* 49 (8) (Aug): 577-81.

Lefranc, F., J. Brotchi, and R. Kiss. 2005. Possible future issues in the treatment of glioblastomas: Special emphasis on cell migration and the resistance of migrating glioblastoma cells to apoptosis. *Journal of Clinical Oncology : Official Journal of the American Society of Clinical Oncology* 23 (10) (Apr 1): 2411-22.

Liang, Y., M. Diehn, N. Watson, A. W. Bollen, K. D. Aldape, M. K. Nicholas, K. R. Lamborn, et al. 2005. Gene expression profiling reveals molecularly and clinically distinct subtypes of glioblastoma multiforme. *Proceedings of the National Academy of Sciences of the United States of America* 102 (16) (Apr 19): 5814-9.

Louis, D. N., H. Ohgaki, O. D. Wiestler, W. K. Cavenee, P. C. Burger, A. Jouvet, B. W. Scheithauer, and P. Kleihues. 2007. The 2007 WHO classification of tumours of the central nervous system. *Acta Neuropathologica* 114 (2) (Aug): 97-109.

Luqmani, Y. A. 2005. Mechanisms of drug resistance in cancer chemotherapy. *Medical Principles and Practice : International Journal of the Kuwait University, Health Science Centre* 14 Suppl 1 : 35-48.

Maher, E. A., and A. C. McKee. 2010. Neoplasms of the central nervous system. in: Skarin AT, canellos GP, eds. atlas of diagnostic oncology, 3rd edition. london, united kingdom: Elsevier science ltd publishers. In , eds. A. T. Skarin, G. P. Canellos. 3rd ed., 484-527. London, United Kingdom: Elsevier Science Ltd.

Marinkovic, N. S., R. Huang, P. Bromberg, M. Sullivan, J. Toomey, L. M. Miller, E. Sperber, et al. 2002. Center for synchrotron biosciences' U2B beamline: An international resource for biological infrared spectroscopy. *Journal of Synchrotron Radiation* 9 (Pt 4) (Jul 1): 189-97.

Martinez, R., W. Roggendorf, G. Baretton, R. Klein, G. Toedt, P. Lichter, G. Schackert, and S. Joos. 2007. Cytogenetic and molecular genetic analyses of giant cell glioblastoma multiforme reveal distinct profiles in giant cell and non-giant cell subpopulations. *Cancer Genetics and Cytogenetics* 175 (1) (May): 26-34.

Mason, W. P., R. D. Maestro, D. Eisenstat, P. Forsyth, D. Fulton, N. Laperriere, D. Macdonald, J. Perry, B. Thiessen, and Canadian GBM Recommendations Committee. 2007. Canadian recommendations for the treatment of glioblastoma multiforme. *Current Oncology (Toronto, Ont.)* 14 (3) (Jun): 110-7.

McIntosh, L. M., M. Jackson, H. H. Mantsch, M. F. Stranc, D. Pilavdzic, and A. N. Crowson. 1999. Infrared spectra of basal cell carcinomas are distinct from non-tumor-bearing skin components. *The Journal of Investigative Dermatology* 112 (6) (Jun): 951-6.

Miller, L. M., and P. Dumas. 2006. Chemical imaging of biological tissue with synchrotron infrared light. *Biochimica Et Biophysica Acta* 1758 (7) (Jul): 846-57.

Miura, M., H. Blattmann, E. Brauer-Krisch, A. Bravin, A. L. Hanson, M. M. Nawrocky, P. L. Micca, D. N. Slatkin, and J. A. Laissue. 2006. Radiosurgical palliation of aggressive murine SCCVII squamous cell carcinomas using synchrotron-generated X-ray microbeams. *The British Journal of Radiology* 79 (937) (Jan): 71-5.

Mohiuddin, M., M. Fujita, W. F. Regine, A. S. Megooni, G. S. Ibbott, and M. M. Ahmed. 1999. High-dose spatially-fractionated radiation (GRID): A new paradigm in the management of advanced cancers. *International Journal of Radiation Oncology, Biology, Physics* 45 (3) (Oct 1): 721-7.

Nakamura, H., K. Makino, and J. I. Kuratsu. 2011. Molecular and clinical analysis of glioblastoma with an oligodendroglial component (GBMO). *Brain Tumor Pathology* (Jun 1).

Nettelbeck, H., G. J. Takacs, M. L. Lerch, and A. B. Rosenfeld. 2009. Microbeam radiation therapy: A monte carlo study of the influence of the source, multislit collimator, and beam divergence on microbeams. *Medical Physics* 36 (2) (Feb): 447-56.

Prezado, Y., S. Thengumpallil, M. Renier, and A. Bravin. 2009. X-ray energy optimization in minibeam radiation therapy. *Medical Physics* 36 (11) (Nov): 4897-902.

Raizer, J. 2011. Issues in developing drugs for primary brain tumors: Barriers and toxicities. *Toxicologic Pathology* 39 (1): 152-7.

Regnard, P., G. Le Duc, E. Brauer-Krisch, I. Tropres, E. A. Siegbahn, A. Kusak, C. Clair, et al. 2008. Irradiation of intracerebral 9L gliosarcoma by a single array of microplanar x-ray beams from a synchrotron: Balance between curing and sparing. *Physics in Medicine and Biology* 53 (4) (Feb 21): 861-78.

Reifenberger, G., and P. Wesseling. 2010. Molecular diagnostics of brain tumors. *Acta Neuropathologica* 120 (5) (Nov): 549-51.

Serduc, R., A. Bouchet, E. Brauer-Krisch, J. A. Laissue, J. Spiga, S. Sarun, A. Bravin, et al. 2009. Synchrotron microbeam radiation therapy for rat brain tumor palliation-influence of the microbeam width at constant valley dose. *Physics in Medicine and Biology* 54 (21) (Nov 7): 6711-24.

Sheleg, S. V., E. A. Korotkevich, E. A. Zhavrid, G. V. Muravskaya, A. F. Smeyanovich, Y. G. Shanko, T. L. Yurkshtovich, P. B. Bychkovsky, and S. A. Belyaev. 2002. Local chemotherapy with cisplatin-depot for glioblastoma multiforme. *Journal of Neuro-Oncology* 60 (1) (Oct): 53-9.

Steiner, G., A. Shaw, L. P. Choo-Smith, M. H. Abuid, G. Schackert, S. Sobottka, W. Steller, R. Salzer, and H. H. Mantsch. 2003. Distinguishing and grading human gliomas by IR spectroscopy. *Biopolymers* 72 (6): 464-71.

Tanaka, G., Y. Nakazato, T. Irie, T. Okada, and M. Abe. 2011. Indeterminacy in the WHO classification of tumors: An example of the histopathological diagnosis of brain tumors. *Brain Tumor Pathology* (Mar 11)[Epub ahead of print].

Tenzel, W. V. 1952. Experience with grid therapy. *Radiology* 59 (3) (Sep): 399-408.

Tobin, M. J., M. A. Chesters, J. M. Chalmers, F. J. Rutten, S. E. Fisher, I. M. Symonds, A. Hitchcock, R. Allibone, and S. Dias-Gunasekara. 2004. Infrared microscopy of epithelial cancer cells in whole tissues and in tissue culture, using synchrotron radiation. *Faraday Discussions* 126 : 27-39.

Valle-Folgueral, J. M., L. Mascarenhas, J. A. Costa, F. Vieira, J. Soares-Fernandes, P. Beleza, and C. Alegria. 2008. Giant cell glioblastoma: Review of the literature and illustrated case. *Neurocirugia (Asturias, Spain)* 19 (4) (Aug): 343-9.

Walker, C., D. G. du Plessis, K. A. Joyce, Y. Machell, J. Thomson-Hehir, S. A. Al Haddad, J. C. Broome, and P. C. Warnke. 2003. Phenotype versus genotype in gliomas displaying inter- or intratumoral histological heterogeneity. *Clinical Cancer Research*

:An Official Journal of the American Association for Cancer Research 9 (13) (Oct 15): 4841-51.

Wieczorek, T., and J. A. Longtine. 2010. The role of molecular probes and other markers in the diagnosis of malignancy. atlas of diagnostic oncology. In , eds. A. T. Skarin, G. P. Canellos. 4th ed., 1-5Mosby Elsevier Publishers.

Wiltshire, R. N., B. K. Rasheed, H. S. Friedman, A. H. Friedman, and S. H. Bigner. 2000. Comparative genetic patterns of glioblastoma multiforme: Potential diagnostic tool for tumor classification. *Neuro-Oncology* 2 (3) (Jul): 164-73.

Wysokinski, T. W., D. Chapman, G. Adams, M. Renier, P. Suortti, and W. Thomlinson. 2007. Beamlines of the biomedical imaging and therapy facility at the canadian light source--part 1. *Nuclear Instruments and Methods in Physics Research Section A: Accelerators, Spectrometers, Detectors and Associated Equipment* 582 (1): 73-6.

Zuber, M. A., W. Krupp, H. Holland, and U. G. Froster. 2002. Characterization of chromosomal aberrations in a case of glioblastoma multiforme combining cytogenetic and molecular cytogenetic techniques. *Cancer Genetics and Cytogenetics* 138 (2) (Oct 15): 111-5.

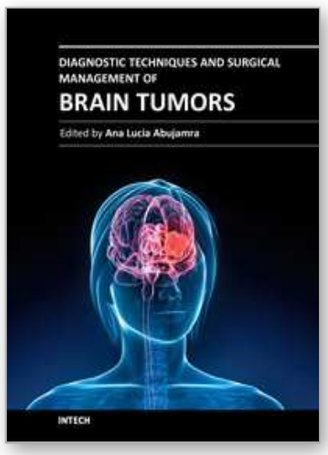

Diagnostic Techniques and Surgical Management of Brain Tumors
Edited by Dr. Ana Lucia Abujamra

ISBN 978-953-307-589-1
Hard cover, 544 pages
Publisher InTech
Published online 22, September, 2011
Published in print edition September, 2011

The focus of the book Diagnostic Techniques and Surgical Management of Brain Tumors is on describing the established and newly-arising techniques to diagnose central nervous system tumors, with a special focus on neuroimaging, followed by a discussion on the neurosurgical guidelines and techniques to manage and treat this disease. Each chapter in the Diagnostic Techniques and Surgical Management of Brain Tumors is authored by international experts with extensive experience in the areas covered.

How to reference
In order to correctly reference this scholarly work, feel free to copy and paste the following:

S. Kaiser Ali, Umashankar Das, Yanjie Lu, Vijayanada Kundapur and Tim May (2011). Synchrotron Radiation: Applications in Diagnosis and Treatment of Malignant Brain Tumors, Diagnostic Techniques and Surgical Management of Brain Tumors, Dr. Ana Lucia Abujamra (Ed.), ISBN: 978-953-307-589-1, InTech, Available from: http://www.intechopen.com/books/diagnostic-techniques-and-surgical-management-of-brain-tumors/synchrotron-radiation-applications-in-diagnosis-and-treatment-of-malignant-brain-tumors

INTECH
open science | open minds

InTech Europe
University Campus STeP Ri
Slavka Krautzeka 83/A
51000 Rijeka, Croatia
Phone: +385 (51) 770 447
Fax: +385 (51) 686 166
www.intechopen.com

InTech China
Unit 405, Office Block, Hotel Equatorial Shanghai
No.65, Yan An Road (West), Shanghai, 200040, China
中国上海市延安西路65号上海国际贵都大饭店办公楼405单元
Phone: +86-21-62489820
Fax: +86-21-62489821

IntechOpen